

Article

Epitaxial Growth of Hard Ferrimagnetic Mn_3Ge Film on Rhodium Buffer Layer

Atsushi Sugihara, Kazuya Suzuki, Terunobu Miyazaki and Shigemi Mizukami *

WPI-Advanced Institute for Materials Research, Tohoku University, Katahira 2-1-1, Sendai 980-8577, Japan; E-Mails: a.sugihara@wpi-aimr.tohoku.ac.jp (A.S.); kazuya.suzuki.fw@wpi-aimr.tohoku.ac.jp (K.S.); miyazaki@wpi-aimr.tohoku.ac.jp (T.M.)

* Author to whom correspondence should be addressed; E-Mail: mizukami@wpi-aimr.tohoku.ac.jp; Tel.: +81-22-217-6003.

Academic Editor: Jordi Sort Vinas

Received: 23 April 2015 / Accepted: 21 May 2015 / Published: 2 June 2015

Abstract: Mn_3Ge has a tetragonal Heusler-like $D0_{22}$ crystal structure, exhibiting a large uniaxial magnetic anisotropy and small saturation magnetization due to its ferrimagnetic spin structure; thus, it is a hard ferrimagnet. In this report, epitaxial growth of a Mn_3Ge film on a Rh buffer layer was investigated for comparison with that of a film on a Cr buffer layer in terms of the lattice mismatch between Mn_3Ge and the buffer layer. The film grown on Rh had much better crystalline quality than that grown on Cr, which can be attributed to the small lattice mismatch. Epitaxial films of Mn_3Ge on Rh show somewhat small coercivity ($H_c = 12.6$ kOe) and a large perpendicular magnetic anisotropy ($K_u = 11.6$ Merg/cm³), comparable to that of the film grown on Cr.

Keywords: spintronics; hard magnetic materials; epitaxial film; magnetic properties; high coercivity

1. Introduction

Magnetism in Mn-based alloys and compounds has been studied, and various types of Mn-based alloys and compounds are known to exist. Among them, to our knowledge, are four types of hard magnetic Mn-based alloys and compounds that show strong ferro/ferrimagnetism with both a high Curie temperature and high uniaxial magnetic anisotropy in their bulk forms. These are categorized in terms of

their crystal structures as follows: (a) Tetragonal $L1_0$ -type crystal structure, for example, MnAl [1,2] and MnGa [3] (Figure 1a); (b) Tetragonal $D0_{22}$ -type crystal structure, for example, Mn_3Ga [4,5] and Mn_3Ge [6–8] (Figure 1b); (c) Tetragonal $C38$ -type crystal structure, for example, MnAlGe [9] (Figure 1c); and (d) Hexagonal $B8_1$ -type crystal structure, for example, MnBi [10,11] (Figure 1d). The distinct difference between Mn-based magnets and others such as Fe–Pt and Nd–Fe–B is that the former are composed of III and/or IV main group elements, and the latter are composed of heavy transition or rare-earth elements. This fact is important in today’s magnetism-based technology for two reasons. One is related to the development of permanent magnets without critical elements, and the other is related to spintronics applications. Hereafter, we focus on the use of hard magnetic Mn-based alloys for spintronics applications; the other topic regarding Mn-based alloys and compounds is discussed in the reviews [12,13].

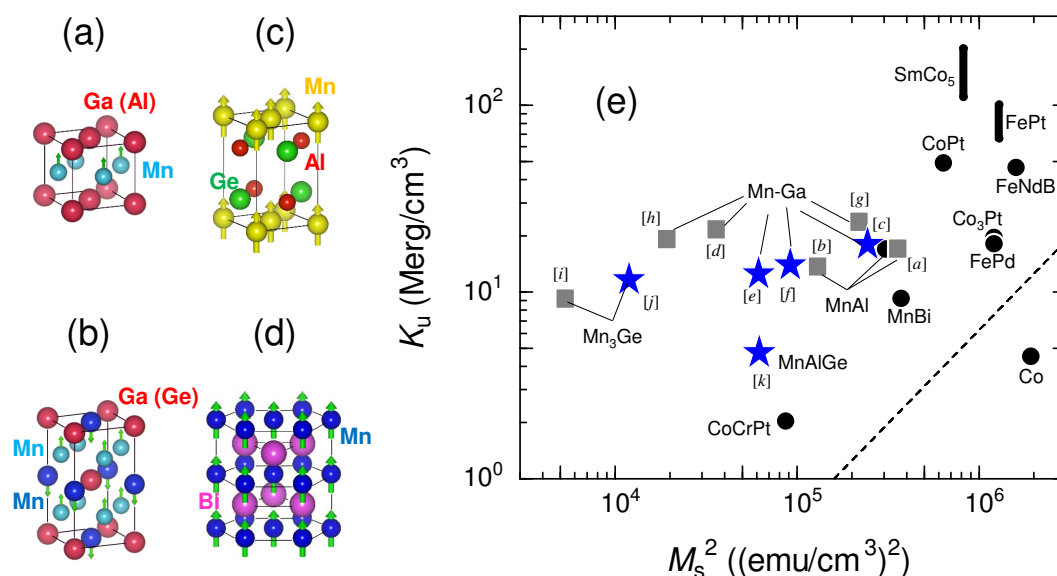


Figure 1. (a) Tetragonal $L1_0$ -type crystal structure, e.g., MnGa and MnAl; (b) Tetragonal $D0_{22}$ -type crystal structure, e.g., Mn_3Ga and Mn_3Ge ; (c) Tetragonal $C38$ -type crystal structure, e.g., MnAlGe; (d) Hexagonal $B8_1$ -type crystal structure, e.g., MnBi; (e) Typical values of K_u as a function of the square of M_s for the c -axis-oriented Mn-based alloy epitaxial films. Solid stars (\star) indicate our data; solid squares indicate other data. Values for conventional hard magnetic materials [11,14] are also shown as solid circles (\bullet). Dashed line indicates the boundary between materials with the magnetic easy axis parallel to the film surface and those with the easy axis perpendicular to the film surface (perpendicular magnetization). References for the data are as follows. [a]: [15]; [b]: [16]; [c]: [17], [d]: [18], [e]: [19], [f]: [17], [g], [h]: [20], [i]: [21], [j]: [22], [k]: [23].

Mn-based hard magnets are very good candidates for magnetic random access memory (MRAM) applications [24,25] because some of them show a small saturation magnetization as well as a large uniaxial magnetic anisotropy. The Gilbert magnetic damping is expected to be smaller than that of hard magnets containing heavy elements because the addition of heavy elements or rare-earth elements to magnetic materials tends to increase the Gilbert damping [25]. For this reason, it is crucial to investigate c -axis-oriented Mn-based hard magnetic films with a high degree of chemical order, as the exchange

interaction between Mn atoms is very sensitive to the environment and the nearest-neighbor distance. This situation is distinct from that of other ordered alloys, such as Fe–Pt, which are ferromagnetic even in disordered states.

Figure 1e shows typical K_u and M_s data from our work and from other groups for *c*-axis-oriented epitaxial films of several Mn-based alloys and the values for conventional hard magnetic materials [14]. The $L1_0$ phase of the Mn–Al binary system is metastable, but epitaxial films were reported recently ([a], [b] in Figure 1e) [15,16]. The $L1_0$ phase of the Mn–Ga binary system is thermodynamically stable at room temperature (RT), and high-quality films have been grown on several types of buffer layers using various techniques ([c], [d] in Figure 1e) [17,18]. The reported values of M_s and K_u for the films are 190–600 emu/cm³ and 13.65–21.7 Merg/cm³, respectively. The $D0_{22}$ phase of the Mn–Ga binary system is also metastable according to recent reports [26], but high-quality epitaxial films can be obtained, as we reported for the first time [19]. The reported values of M_s and K_u for $D0_{22}$ Mn–Ga films are 140–470 emu/cm³ and 12.4–23.5 Merg/cm³, respectively ([e], [f], [g], [h] in Figure 1e) [17,19,20]. Epitaxial films of C38 MnAlGe can be easily grown; their M_s value is 250 emu/cm³, but K_u is small ([k] in Figure 1e) [23].

Quite recently, (001)-oriented epitaxial films of $D0_{22}$ Mn_3Ge have also been reported to show small magnetization of about 73 emu/cm³ and a K_u value of 9.1 Merg/cm³ ([i] in Figure 1e) [21]. Higher-quality films were obtained using a Cr buffer layer and sophisticated control of the Mn composition and growth temperature [22,27]. Films with stoichiometric compositions exhibited a K_u value of 11.8 Merg/cm³ and an M_s value of ~ 110 emu/cm³ ([j] in Figure 1e) [22]. $D0_{22}$ Mn_3Ge is considered to have the properties most suitable for MRAM [28,29], although few examples of epitaxial growth have been reported. In particular, it is unclear how lattice matching between Mn_3Ge and the buffer or substrate affect the magnetic properties of films. For example, films grown on the (001) $SrTiO_3$ substrate, with negligible lattice mismatch, show very broad hysteresis curves with a large coercive force [21], whereas those grown on a Cr buffer layer showed well-squared out-of-plane hysteresis loops and smaller coercivity, even though the lattice mismatch is much greater than that with $SrTiO_3$ [22,27]. In this article, the epitaxial growth of Mn_3Ge films on a Rh buffer layer was investigated, as the lattice constant of Rh is identical to that of Mn_3Ge and we can compare the result with previously reported films grown on a Cr buffer layer in terms of the lattice mismatch between Mn_3Ge and the buffer.

2. Experimental Methods

Samples were prepared on single-crystal MgO (001) substrates by a UHV sputtering apparatus (MPS-3000, Ulvac, Chigasaki, Japan) whose base pressure and work pressure are $<2 \times 10^{-7}$ Pa and ~ 0.1 Pa, respectively. We prepared two types of stacked films having a buffer layer consisting of a Cr single layer or a Cr/Rh bilayer. Before film preparation, the substrates were thermally flushed at 700 °C in the sputtering chamber. Cr layers 40 nm thick were deposited on the substrates at RT and subsequently annealed at 700 °C to form a flat surface. A 20-nm-thick Rh layer was deposited at RT on the Cr layer. Mn_3Ge layers 130 nm thick were deposited by a co-sputtering technique from simple Mn and Ge targets on the substrates with the buffer layers, which were heated at 400 °C. Finally, 3-nm-thick MgO layers were deposited as cap layers. Schematic illustrations of the films are shown in Figure 2. The samples

were characterized according to their surface roughness, crystal structure, magnetization hysteresis curves, and magnetic anisotropy by an *ex-situ* atomic force microscope (AFM) (SII NanoTechnology, SPI-3800N/SPA400, Chiba, Japan), X-ray diffractometer (XRD) (Rigaku, SmartLab, Akishima, Japan), vibrating sample magnetometer, and magnetic torque meter, respectively. All the measurements were conducted at RT and ambient pressure.

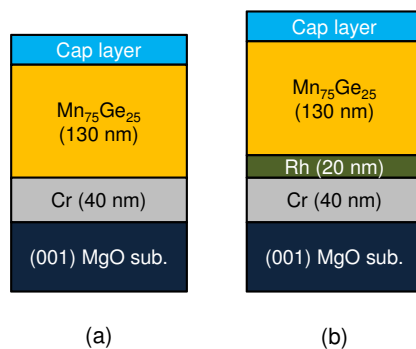


Figure 2. Schematic illustrations of films with (a) Cr and (b) Cr/Rh buffer layer.

3. Experimental Results and Discussion

Figure 3a,b show AFM images of the surfaces of the Cr and Cr/Rh buffer layers, respectively. Both show atomically flat surfaces whose Ra roughness is smaller than 0.2 nm. Figure 3c,d show AFM images of Mn₃Ge layers on the Cr and Cr/Rh buffer layers, respectively. Their roughness is comparable, although the grain sizes differ significantly, which implies a difference in their crystallinity.

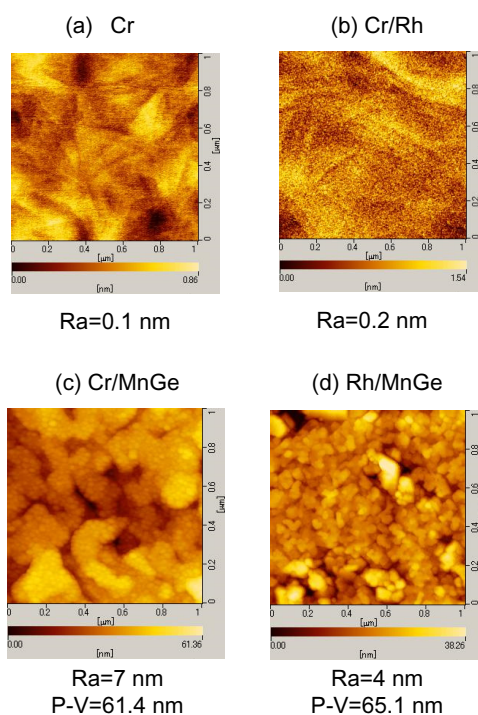


Figure 3. Atomic force microscope (AFM) images of surfaces of (a) Cr buffer layer; (b) Cr/Rh buffer layer; (c) Mn₃Ge on Cr buffer layer; and (d) Mn₃Ge on Cr/Rh buffer layer.

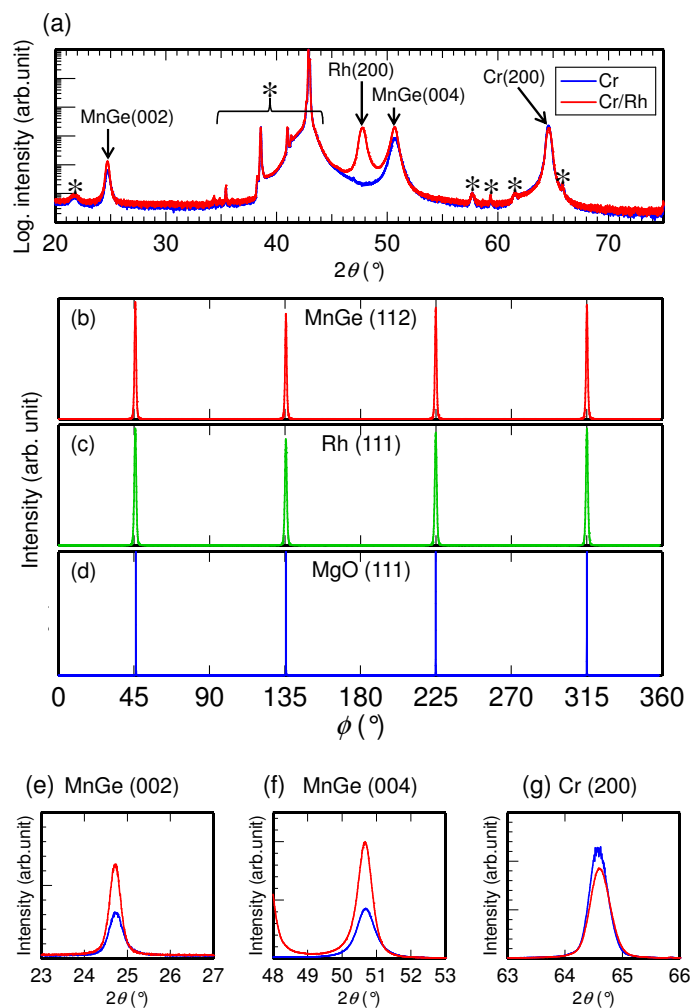


Figure 4. (a) Full X-ray diffractometer (XRD) profiles of films with Cr (blue) and Cr/Rh (red) buffer layers; and the pole figures (ϕ -scan) of (b) $D0_{22}$ - Mn_3Ge (112) (c) Rh (111); and (d) MgO substrate (111); Magnifications of the XRD curve of (e) $D0_{22}$ - Mn_3Ge (002); (f) $D0_{22}$ - Mn_3Ge (004), and (g) Cr (200) peaks.

Figure 4a shows the XRD profiles of the films with Cr and Cr/Rh buffer layers. Peaks marked by asterisks are the background signals, such as those from the substrate and X-ray tube. Only the (200) peaks from Cr and Rh are observed for the films, indicating that both buffer layers are (001)-oriented as a result of epitaxial growth on their MgO (001) substrates. For the Mn_3Ge layer, only the (002) and (004) peaks from $D0_{22}$ -structured Mn_3Ge were observed, which indicated that the Mn_3Ge layers has the $D0_{22}$ structure and a completely (001)-preferred crystallographic orientation. Figure 4b–d show pole figures (ϕ -scans) of Mn_3Ge , Rh, and MgO substrate, and those exhibit the four-fold symmetry. The ϕ value of the (111) peak from the MgO (001) substrate was the same as that of the (112) peak from $D0_{22}$ - Mn_3Ge and the (111) peak from Rh but was shifted by 45° from the (222) peak of Cr (not shown here), indicating the following epitaxial relationship: $MgO[100](001)\parallel Cr[110](001)\parallel Rh[100](001)\parallel D0_{22}-Mn_3Ge[100](001)$. Figure 4e–g show magnified profiles of the Mn_3Ge (002), Mn_3Ge (004), and Cr (200) peaks, respectively. Note that the vertical axis is on a linear scale, whereas that of Figure 4a is on a logarithmic scale. The (002) and (004) peaks from Mn_3Ge for the film with the Cr/Rh buffer layer are significantly more intense than those from the

film with the Cr buffer layer. This indicates that the crystallinity of Mn₃Ge on the Cr/Rh layer is better than that on the Cr buffer layer. Because the intensity of the Cr (200) peak is comparable, the effect of interdiffusion between the Cr and Mn₃Ge layers is absent in the film. Hence, the Cr/Rh buffer layer intrinsically improves the crystallinity of the Mn₃Ge above. This is possibly the result of the reduction in the lattice mismatch between the buffer layer and Mn₃Ge layer due to the presence of Rh. Assuming that the epitaxial distortion in the Rh layer due to the lattice mismatch between Cr ($a = 2.885 \text{ \AA}$ in bulk) and Rh ($a = 3.805 \text{ \AA}$ in bulk) is sufficiently relaxed, the lattice mismatch between the buffer layer and the Mn₃Ge ($a = 3.80 \text{ \AA}$ in bulk) layer is reduced from 6.86% to 0.13% by the Rh layer. Although a flat surface is expected as the result of layer-by-layer growth due to the absence of distortion energy for such a small lattice mismatch, the Mn₃Ge on Rh shows a rough surface whose Ra value is comparable with that of the film on Cr, as shown in the AFM images. The large roughness may be the result of the poor wettability of Rh for Mn₃Ge. The use of a surfactant may be effective for obtaining a smooth surface of Mn₃Ge on the Cr/Rh buffer layer [30,31].

Figure 5 shows magnetization field ($M-H$) curves of Mn₃Ge on Cr and Cr/Rh buffer layers. The saturation magnetization (M_s) for the film with the Cr/Rh buffer layer (115 emu/cm³) is comparable with that for the film with the Cr buffer layer (100 emu/cm³), whereas the former has a lower coercivity ($H_c = 12.6 \text{ kOe}$) than the latter (14.9 kOe). This is consistent with the previously reported experimental results, which suggested that highly crystalline Mn₃Ge has a comparatively high M_s and low H_c [22,27].

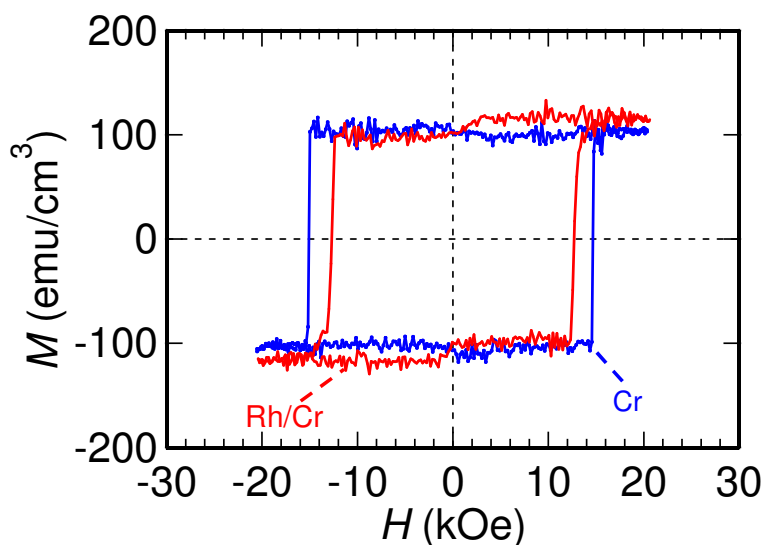


Figure 5. Magnetization field curves for films with Cr (blue) and Cr/Rh (red) buffer layer.

Figure 6a shows the magnetic torque curve of Mn₃Ge with the Cr/Rh buffer layer measured at various applied fields. The curves have a sawtooth-like shape, which indicates that the Mn₃Ge is not magnetically saturated during the measurements. In this case, a special method is needed to estimate the anisotropy constant. We employed the Miyajima method (45° method) [32]. Figure 6b shows plots based on the Miyajima method for the films on the Cr and Cr/Rh buffer layers; their x intercepts give the torque values at an infinite field (completely saturated state). From these plots, the anisotropy constants (K_{us}) are estimated to be 13.2 and 11.6 Merg/cm³ for the films on the Cr and Cr/Rh buffer layers, respectively.

Interestingly, the film on the Cr/Rh buffer layer has a lower K_u value than that on the Cr buffer layer despite its better crystallinity. The origin of this low K_u is not yet clear. One possibility is the difference between the optimal composition of the Mn–Ge layer on the Cr and Cr/Rh layers. Mn–Ge has different optimal compositions for obtaining $D0_{22}$ structure and the best magnetic properties, e.g., $Mn_{3.4}Ge$ in the bulk state [33], $Mn_{3.55}Ge$ in the thin film state on MgO (001) [28], and Mn_3Ge in the thin film state on Cr (001) [22,27]. It may be necessary to optimize the composition of the Mn_3Ge layer to obtain the best magnetic properties on a Cr/Rh buffer layer.

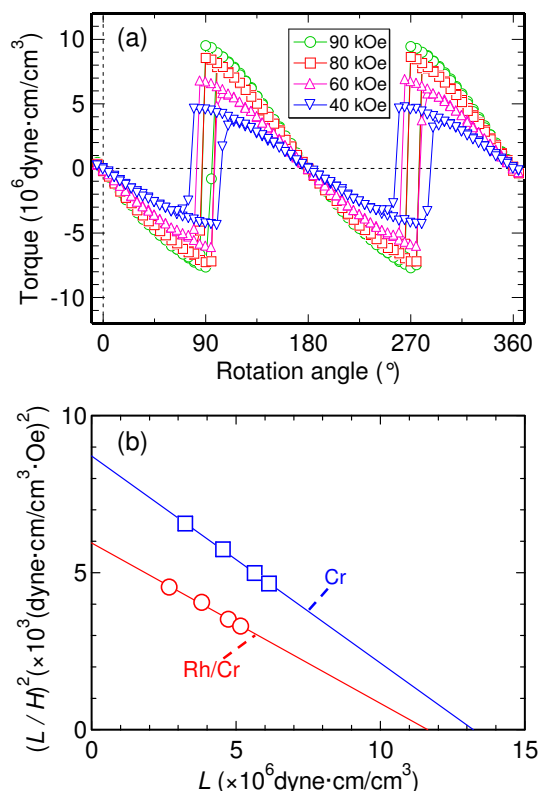


Figure 6. (a) Magnetic torque curves measured at various applied fields for the film with a Cr/Rh buffer layer; (b) Miyajima plot for films with Cr (blue) and Cr/Rh (red) buffer layers.

4. Conclusions

We prepared Mn_3Ge layers on Cr and Cr/Rh buffered MgO (001) substrates and characterized their surface roughness, crystal structure, magnetization field curves, and magnetic anisotropy constants. The crystallinity of the epitaxially grown Mn_3Ge layer on Cr/Rh was better than that of the layer grown on the Cr buffer layer. It was demonstrated that the epitaxial relationship among MgO, Cr, Rh, and Mn_3Ge is $MgO[100](001)\parallel Cr[110](001)\parallel Rh[100](001)\parallel D0_{22}-Mn_3Ge[100](001)$. The saturation magnetization and coercivity obtained from magnetization field curves also suggested that Mn_3Ge on Cr/Rh had better crystallinity than that on Cr. Magnetic torque measurements exhibited that the anisotropy constant of Mn_3Ge on the Cr/Rh buffer layer is comparable to that of the film on the Cr buffer layer despite the better crystallinity of the former.

Acknowledgments

This work was supported in part by the Development of an infrastructure for normally-off computing technology project from NEDO and the Asahi glass foundation.

Author Contributions

A.S. and K.S. performed the experiments. A.S., K.S., T.M., and S.M. discussed the experimental results. A.S. and S.M. wrote the manuscript. All the authors agree with the manuscript.

Conflicts of Interest

The authors declare no conflict of interest.

References

1. Kono, H. On the ferromagnetic phase in manganese-aluminum system. *J. Phys. Soc. Jpn.* **1958**, *13*, 1444–1451.
2. Koch, A.J.J.; Hokkeling, P.; de Vos, K.J. New material for permanent magnets on a base of Mn and Al. *J. Appl. Phys.* **1960**, *31*, S75–S77.
3. Bither, T.A.; Cloud, W.H. Magnetic tetragonal δ phase in the Mn-Ga binary. *J. Appl. Phys.* **1965**, *36*, 1501–1502.
4. Krén, E.; Kádár, G. Neutron diffraction study of Mn_3Ga . *Solid State Commun.* **1970**, *8*, 1653–1655.
5. Niida, H.; Hori, T.; Onodera, H.; Yamaguchi, Y.; Nakagawa, Y. Magnetization and coercivity of $Mn_{3-\delta}Ga$ alloys with a $D0_{22}$ -type structure. *J. Appl. Phys.* **1996**, *79*, 5946–5948.
6. Ohoyama, T.; Yasukochi, K.; Kanematsu, K. A new phase of an intermetallic compound $Mn_{3.4}Ge$ and its magnetism. *J. Phys. Soc. Jpn.* **1961**, *16*, 352–353.
7. Ohoyama, T. X-ray and magnetic studies of the manganese-germanium system. *J. Phys. Soc. Jpn.* **1961**, *16*, 1995–2002.
8. Yamada, N. Atomic magnetic moment and exchange interaction between Mn atoms in intermetallic compounds in Mn-Ge system. *J. Phys. Soc. Jpn.* **1990**, *101*, 273–288.
9. Wernick, J.H.; Haszko, S.E.; Romanow, W.J. New magnetic ternary compound with a high crystalline anisotropy. *J. Appl. Phys.* **1961**, *32*, 2495.
10. Guillaud, C. Hexagonal crystals of $Mn_{3-\delta}I$. Ph.D. Thesis, University of Strasbourg, Strasbourg, France, 1943.
11. Williams, H.J.; Sherwood, R.C.; Boothby, O.L. Magnetostriction and magnetic anisotropy of MnBi. *J. Appl. Phys.* **1957**, *28*, 445–447.
12. Zhu, L.; Zhao, J. Perpendicularly magnetized Mn_xGa films: Promising materials for future spintronic devices, magnetic recording and permanent magnets. *Appl. Phys. A* **2013**, *111*, 379–387.
13. Coey, J.M.D. New permanent magnets; manganese compounds. *J. Phys. Condens. Matter* **2014**, *26*, 064211-1–064211-6.
14. Weller, D.; Moser, A.; Folks, L.; Best, M.E.; Lee, W.; Toney, M.F.; Schwickert, M.; Thiele, J.-U.; Doerner, M.F. High K_u materials approach to 100 Gbits/in². *IEEE Trans. Magn.* **2000**, *36*, 10–15.

15. Hosoda, M.; Oogane, M.; Kubota, M.; Kubota, T.; Saruyama, H.; Iihama, S.; Naganuma, H.; Ando, Y. Fabrication of $L1_0$ -MnAl perpendicularly magnetized thin films for perpendicular magnetic tunnel junctions. *J. Appl. Phys.* **2012**, *111*, 07A324-1–07A324-3.
16. Nie, S.H.; Zhu, L.J.; Lu, J.; Pan, D.; Wang, H.L.; Yu, X.Z.; Xiao, J.X.; Zhao, J.H. Perpendicularly magnetized τ -MnAl (001) thin films epitaxied on GaAs. *Appl. Phys. Lett.* **2013**, *102*, 152405-1–152405-4.
17. Mizukami, S.; Wu, F.; Sakuma, A.; Walowski, J.; Watanabe, D.; Kubota, T.; Zhang, X.; Naganuma, H.; Oogane, M.; Ando, Y.; *et al.* Long-lived ultrafast spin precession in manganese alloys films with a large perpendicular magnetic anisotropy. *Phys. Rev. Lett.* **2011**, *106*, 117201-1–117201-4.
18. Zhu, L.; Nie, S.; Meng, K.; Pan, D.; Zhao, J.; Zheng, H. Multifunctional $L1_0$ -Mn_{1.5}Ga films with ultrahigh coercivity, giant perpendicular magnetocrystalline anisotropy and large magnetic energy product. *Adv. Mater.* **2012**, *24*, 4547–4551.
19. Wu, F.; Mizukami, S.; Watanabe, D.; Naganuma, H.; Oogane, M.; Ando, Y.; Miyazaki, T. Epitaxial Mn_{2.5}Ga thin films with giant perpendicular magnetic anisotropy for spintronic devices. *Appl. Phys. Lett.* **2009**, *94*, 122503-1–122503-3.
20. Kurt, H.; Rode, K.; Venkatesan, M.; Stamenov, P.; Coey, J.M.D. Mn_{3-x}Ga ($0 \leq x \leq 1$): Multifunctional thin film materials for spintronics and magnetic recording. *Phys. Status Solidi B* **2011**, *248*, 2338–2344.
21. Kurt, H.; Baadji, N.; Rode, K.; Venkatesan, M.; Stamenov, P.; Sanvito, S.; Coey, J.M.D. Magnetic and electronic properties of D0₂₂-Mn₃Ge (001) films. *Appl. Phys. Lett.* **2012**, *101*, 132410-1–132410-3.
22. Sugihara, A.; Mizukami, S.; Yamada, Y.; Koike, K.; Miyazaki, T. High perpendicular magnetic anisotropy in D0₂₂-Mn_{3+x}Ge tetragonal Heusler alloy films. *Appl. Phys. Lett.* **2014**, *104*, 132404-1–132404-4.
23. Mizukami, S.; Sakuma, A.; Kubota, T.; Kondo, Y.; Sugihara, A.; Miyazaki, T. Fast magnetization precession for perpendicularly magnetized MnAlGe epitaxial films with atomic layered structures. *Appl. Phys. Lett.* **2013**, *103*, 142405-1–142405-4.
24. Yoda, H.; Kishi, T.; Nagase, T.; Yoshikawa, M.; Nishiyama, K.; Kitagawa, E.; Daibou, T.; Amano, M.; Shimomura, N.; Takahashi, S.; *et al.* High efficient spin transfer torque writing on perpendicular magnetic tunnel junctions for high density MRAMs. *Curr. Appl. Phys.* **2010**, *10*, e87–e89.
25. Ma, Q.; Sugihara, A.; Suzuki, K.; Zhang, X.; Miyazaki, T.; Mizukami, S. Tetragonal Heusler-like Mn-Ga alloys based perpendicular magnetic tunnel junctions. *Spin* **2014**, *4*, 1440024-1–1440024-14.
26. Minakuchi, K.; Umetsu, R.Y.; Ishida, K.; Kainuma, R. Phase equilibria in the Mn-rich portion of Mn-Ga binary system. *J. Alloys Compd.* **2012**, *537*, 332–337.
27. Sugihara, A.; Suzuki, K.Z.; Miyazaki, T.; Mizukami, S. Structure and magnetic properties of tetragonal Heusler D0₂₂ Mn₃Ge compound epitaxial films with high perpendicular magnetic anisotropy. *J. Phys. D* **2015**, *48*, 164009-1–164009-5.

28. Mizukami, S.; Sakuma, A.; Sugihara, A.; Kubota, T.; Kondo, Y.; Tsuchiura, H.; Miyazaki, T. Tetragonal $D0_{22}$ $Mn_{3+x}Ge$ epitaxial films grown on MgO(100) with a large perpendicular magnetic anisotropy. *Appl. Phys. Express* **2013**, *6*, 123002-1–123002-4.
29. Miura, Y.; Shirai, M. Theoretical study on tunneling magnetoresistance of magnetic tunnel junctions with $D0_{22}$ - Mn_3Z ($Z = Ga, Ge$). *IEEE. Trans. Magn.* **2014**, *50*, 1400504-1–1400504-4.
30. Van der Vegt, H.A.; van Pinxteren, H.M.; Lohmeier, M.; Vlieg, E. Surfactant-induced layer-by-layer growth of Ag on Ag(111). *Phys. Rev. Lett.* **1992**, *68*, 3335–3338.
31. Esch, S.; Hohage, M.; Michely, T.; Comsa, G. Origin of oxygen induced layer-by-layer growth in homoepitaxy on Pt(111). *Phys. Rev. Lett.* **1994**, *72*, 518–521.
32. Miyajima, H.; Sato, K.; Mizoguchi, T. Simple analysis of torque measurement of magnetic thin films. *J. Appl. Phys.* **1974**, *47*, 4669–4671.
33. Gokhale, A.B.; Abbaschian, R. The Ge-Mn (Germanium-Manganese) system. *Bull. Alloy Phase Diagr.* **1990**, *11*, 460–468.

© 2015 by the authors; licensee MDPI, Basel, Switzerland. This article is an open access article distributed under the terms and conditions of the Creative Commons Attribution license (<http://creativecommons.org/licenses/by/4.0/>).